Materials Transactions, Vol. 50, No. 8 (2009) pp. 2079 to 2086

EXPRESS REGULAR ARTICLE

Tailoring Thermally Induced Nano-Quasicrystallization and Deformation-Assisted Nanocrystallization for Mechanical Property Improvement in Zr-Al-Ni-Cu-Pd Bulk Metallic Glasses

Junji Saida[1,*], Albertus D. Setyawan[1], Hidemi Kato[2], Mitsuhide Matsushita[3] and Akihisa Inoue[4]

[1]*Center for Interdisciplinary Research, Tohoku University, Sendai 980-8578, Japan*
[2]*Institute for Materials Research, Tohoku University, Sendai 980-8577, Japan*
[3]*Advanced Technology Division, JEOL Ltd., Tokyo 196-8558, Japan*
[4]*WPI-Advanced Institute for Materials Research, Tohoku University, Sendai 980-8577, Japan*

The material design tailoring of a synergistic effect of an *in-situ* nano secondary phase formation and deformation-induced nanocrystallization for improving the mechanical strength and ductility, has been investigated in $Zr_{65}Al_{7.5}Ni_{10}Cu_{17.5-x}Pd_x$ bulk metallic glasses (BMGs). As-cast $Zr_{65}Al_{7.5}Ni_{10}Cu_{17.5-x}Pd_x$ ($x = 5$–17.5) BMGs have significant ductility in compressive deformation, which is attributed to deformation-induced dynamic nanocrystallization. The 10 at% Pd-containing BMG with a low volume fraction of the quasicrystalline (QC) phase of less than 6% exhibits increases in strength and Young's modulus, in addition to a remaining plasticity of ~5%, compared with the monolithic glassy alloy. Such improvements in the mechanical properties originate from the combination of two effects of *in-situ* homogeneous nano-QC formation and deformation-induced inhomogeneous nanocrystallization. The present method should be regarded as a new technique for the production of BMGs with high strength and good ductility. [doi:10.2320/matertrans.M2009135]

(Received April 14, 2009; Accepted May 21, 2009; Published July 8, 2009)

Keywords: *metallic glasses, nanostructure, quasicrystals, nanocomposite, ductility, deformation-induced nanocrystallization*

1. Introduction

Bulk metallic glasses (BMGs) are considered to be exceptional structural materials owing to their attractive mechanical properties, such as a high strength approaching the theoretical value, high elastic energy storage per unit volume, high hardness, low mechanical damping and high fracture toughness.[1,2] The materials, however, generally exhibit poor room-temperature ductility, which prevents them from being used in some engineering applications. Nevertheless, recently, there have been a number of works reporting BMGs or BMG composites with improved ductility. Explanations for the origin of ductility were proposed: (1) a large Poisson's ratio,[3] (2) the presence of heterogeneity and/or short-/medium-range order,[4,5] (3) liquid-liquid phase separation,[6] (4) large free volume,[7,8] (5) introduced porosity,[9,10] (6) introduced *in-situ* secondary phase[11,12] or *ex-situ* foreign particles,[13–15] and (7) crystallization during deformation.[16–19] In most cases, improved mechanical properties were achieved by applying one method but little was reported about the synergistic effect of two or more of the factors mentioned above on the development of the mechanical properties of BMGs.

In this work, we attempt to tailor the alloy design and synthesis for the combination of two factors, the *in-situ* nano secondary phase formation and dynamic nanocrystallization during deformation in BMGs. We have already reported a significant plasticity owing to the deformation-induced dynamic nanocrystallization in the $Zr_{65}Al_{7.5}Ni_{10}Pd_{17.5}$ BMG.[16] The Zr-Al-Ni-Cu-Pd metallic glass is also a well-known nano-quasicrystalline (QC) phase-forming alloy prepared by static annealing near its crystallization temperature, and a considerable improvement of mechanical strength is achieved by nano-QC formation in the glassy matrix.[20,21] In the present paper, we have investigated a new approach for the development of BMGs through the combination of static and dynamic structure control and succeeded in forming a new BMG with high strength and good ductility. Based on the obtained results, we propose a new technique for the development of BMGs using the synergistic effect by the optimization of alloy design and structure control.

2. Experimental Procedure

Master ingots of $Zr_{65}Al_{7.5}Ni_{10}Cu_{17.5-x}Pd_x$ ($x = 0$, 5, 10, 12.5, 15, 17.5 at%) alloys were prepared by arc melting mixtures of pure elements (99.9 mass% Zr, 99.99 mass% Al, 99.9% Ni, 99.99 mass% Cu and 99.9 mass% Pd) in an argon atmosphere. Glassy rods 2.5 mm in diameter and 50 mm in length were fabricated by copper-mold casting, applying an ambient Ar atmosphere pressure in the casting chamber in order to suppress the precipitation of the QC phase.[22] The glassy nature of specimens was verified by X-ray diffractometry (XRD) with Cu-Kα radiation. Thermal stability of specimens was examined by differential scanning calorimetry (DSC). For the compressive test, cylindrical specimens with the dimensions (diameter × length) of 2.5×5 mm were prepared from the glassy rods, and some of them were subjected to pre-annealing in a vacuum atmosphere. The compressive test was performed on 6-10 specimens at room temperature at the strain rate of $5 \times 10^{-4}\ s^{-1}$ using an Instron-type mechanical testing machine. To avoid the geometry effect on the deformation behavior,[23] both ends of the specimen surfaces were polished carefully prior to the test so that they were parallel to each other and perpendicular to the compression axis. The fracture morphology was examined by scanning electron microscopy (SEM) with an

*Corresponding author, E-mail: jsaida@cir.tohoku.ac.jp

accelerating voltage of 20 kV. The microstructure of as-solidified and as-annealed specimens and their fracture surfaces was observed by transmission electron microscopy (TEM) using a field-emission-type microscope (JEOL, JEM-3000F) with an accelerating voltage of 300 kV.

3. Results

3.1 Thermal stability and mechanical properties of as-cast Zr-Al-Ni-Cu-Pd BMGs

Figure 1 shows typical DSC curves of the glassy $Zr_{65}Al_{7.5}Ni_{10}Cu_{17.5-x}Pd_x$ ($x = 0$, 5, 10, 12.5, 15, 17.5 at%) alloys. The $x = 0$ alloy exhibits a single exothermic peak in addition to a large supercooled-liquid (SCL) region of $\Delta T_x = 104$ K ($\Delta T_x = T_x - T_g$, where T_x and T_g are the crystallization and glass-transition temperatures, respectively). In fact, this is a well-known highly glass-formable Zr-based alloy developed in the last decade.[24] The exothermic peak belongs to the decomposition of glass into stable crystalline phases, i.e., Zr_2Cu, Zr_2Ni, Zr_2Al_3 and ZrNi.[21] Partial substitution of Cu with Pd leads to a decrease of ΔT_x from 104 K (in the $x = 0$ alloy) to 68 K in the $x = 5$ alloy. In addition, the single exothermic peak after the SCL region splits into two-stage exothermic ones in the Pd-containing alloys. The first peak corresponds to the precipitation of a nanoscale icosahedral QC phase from the glassy phase, while the second one corresponds to the decomposition of the nano-QC to stable crystalline phases, such as tetragonal-Zr_2Ni, Zr_2Cu and Zr_2Al_3.[21] Increasing x to 10 at% makes the SCL state much less stable as ΔT_x decreases to 48 K, and this value does not change so much (in the range of 40–48 K) when $x =$ 10–17.5 at%. A conspicuous change is seen in the temperature span between the first and second exothermic peaks; the peak-temperature span apparently widens with increasing x, indicating that the first exothermic reaction or precipitation of the nano-QC phase is stabilized upon Pd addition.

Figure 2 displays engineering stress-strain (S-S) curves of the as-cast $Zr_{65}Al_{7.5}Ni_{10}Cu_{17.5-x}Pd_x$ BMGs. The mechanical properties, together with the thermal properties, are summarized in Table 1. It is clear that the yield strength (σ_y) and Young's modulus are in the range of 1500–1600 MPa and 84–86 GPa, respectively, and do not greatly vary among the alloys. The compressive plastic strain (ε_p), however, is clearly different between Pd-containing and non-Pd-containing alloys, as it is only ~1.4% for the $x = 0$ alloy but becomes 5–7% in the $x = 5$–17.5 alloys. A different feature in the fracture morphology is also seen between the samples exhibiting slight and large plasticity. Typically, fine vein patterns and multiple shear bands are observed in the SEM images of the fracture and lateral surfaces of the samples exhibiting large plasticity, as shown in Figs. 3(c)–(f), i.e., in the $x = 5$ and $x = 10$ alloys. On the other hand, the vein pattern in the fracture surface of the $x = 0$ alloy (low

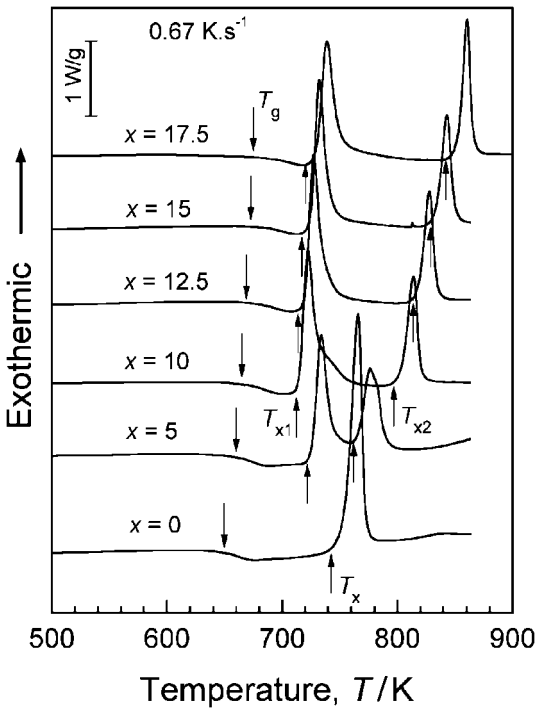

Fig. 1 Typical DSC curves of as-cast $Zr_{65}Al_{7.5}Ni_{10}Cu_{17.5-x}Pd_x$ ($x = 0$, 5, 10, 12.5, 15, 17.5 at%) BMGs.

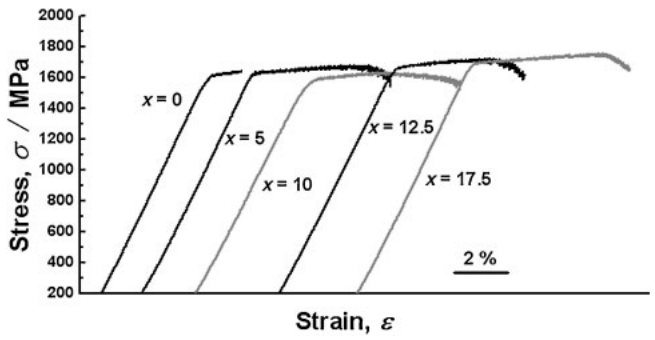

Fig. 2 Engineering stress-strain (S-S) curves of as-cast $Zr_{65}Al_{7.5}Ni_{10}Cu_{17.5-x}Pd_x$ ($x = 0$, 5, 10, 12.5, 17.5 at%) BMGs.

Table 1 Thermal analysis data and mechanical properties of $Zr_{65}Al_{7.5}Ni_{10}Cu_{17.5-x}Pd_x$ BMGs.

Pd content, x (at%)	T_g (K)	T_{x1} (K)	T_{x2} (K)	ΔT_g (K)	σ_y (MPa)	σ_{max} (MPa)	E (GPa)	$\varepsilon_{pl.}$ (%)
0	648	752	—	104	1582	1675	85	1.4
5	657	725	765	68	1530	1643	84	6.0
10	669	715	802	46	1501	1623	85	5.7
12.5	676	719	817	43	1587	1668	86	5.0
15	684	724	833	40	1641	1688	86	6.0
17.5	689	730	851	41	1582	1689	86	6.9

T_g: glass transition temperature; T_{x1}, T_{x2}: onset temperature of the 1st and 2nd crystallization peaks $\Delta T_g = T_{x1} - T_g$; σ_y: yield strength; σ_{max}: maximum strength; E: Young's modulus; $\varepsilon_{pl.}$: plastic strain

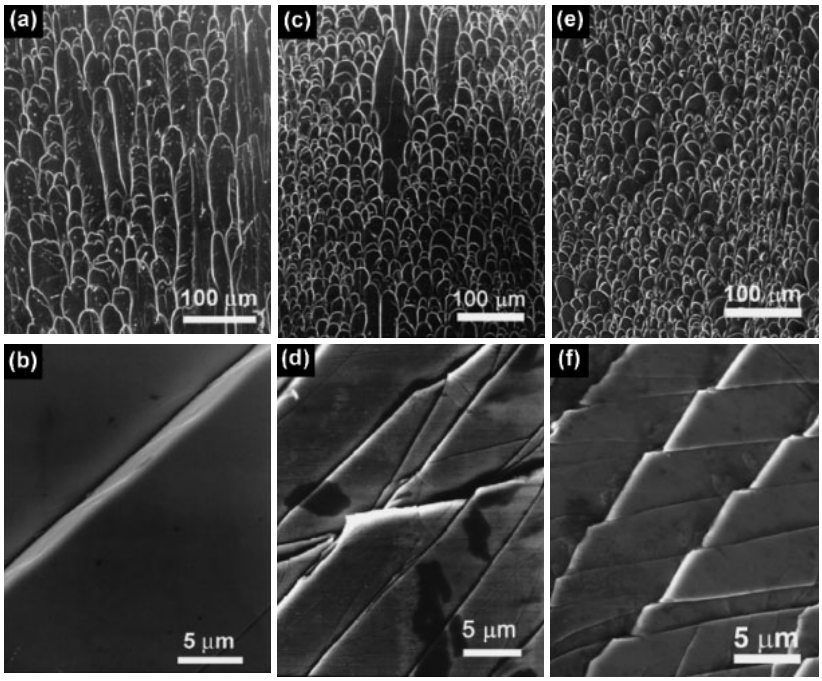

Fig. 3 SEM images of fracture and lateral surfaces of $Zr_{65}Al_{7.5}Ni_{10}Cu_{17.5-x}Pd_x$ BMGs. ((a), (b): $x = 0$, (c), (d): $x = 5$, (e), (f): $x = 10$).

plasticity) is relatively rough (Fig. 3(a)) and almost no evidence of multi-shear-band interaction was observed in the lateral surface (Fig. 3(b)).

3.2 Deformation-induced nanocrystallization: origin of plasticity

In order to understand the origin of the plasticity of BMGs (particularly for $x = 5$–17.5 at%), a thorough TEM observation was performed on both the as-cast and the deformed samples. No clue was found in the microstructure of the as-cast samples (not shown here) for all alloys in this state, which have a monolithic glassy structure. The deformed samples, however, show different results. Figures 4(a)–(h) represent high-resolution TEM (HREM) images and selected-area diffraction patterns (SADPs) taken from the fracture surface of $x = 0$, 5, 10 and 17.5 alloys. The direction of TEM observation is perpendicular to the fracture surface. The fracture surface of the $x = 0$ alloy contains no fringe contrast in the HREM image and a halo ring in the SADP (Figs. 4(a) and (b)), suggesting that no microstructural change is detected during deformation. In contrast, a unique microstructure consisting of a nanoscale "band-like" pattern is observed in the HREM images of the $x = 5$, 10 and 17.5 alloys. The SADPs taken from each sample contain some diffraction spots, which indicate a microstructural change from the fully amorphous structure during deformation. A magnified HREM (Fig. 4(i)) image taken from the fracture surface of the $x = 5$ alloy (shown in Fig. 4(c)) reveals the existence of some nanoparticles (denoted as "NC") with diameters of 5–10 nm in the dark region of the band-like structure, while a typical homogenous maze contrast of the glassy phase is observed in the bright region. Similar images consisting of nanocrystalline particles in the dark region and homogeneous glassy structure in the bright region are confirmed in other fractured BMGs with $x = 10$ and 17.5. Considering the direction of TEM observation, the shear band would propagate in the direction of arrow indicated in Fig. 4(g). The nanoparticles are identified as the metastable fcc-Zr_2Ni phase from the nanobeam diffraction (NBD) pattern shown in Fig. 4(j). An enlarged image of the "NC" region involves two fringe contrasts with spacings of 0.187 nm and 0.239 nm in Fig. 4(k), corresponding to the (622) and (333) interplanar spacings of fcc-Zr_2Ni, respectively. The fcc-Zr_2Ni phase is known to be a unique structure containing the distorted icosahedral cluster in the large unit cell with the lattice parameter of approximately $a = 1.23$ nm.[25,26]

The mechanical properties, particularly the plasticity, of the $Zr_{65}Al_{7.5}Ni_{10}Cu_{17.5-x}Pd_x$ BMGs certainly correlate to the microstructural change observed between the as-cast and the deformed states. As the structure remains glassy (thus, no structural changes) during deformation, the $x = 0$ alloy exhibits slight plasticity accompanying a typical catastrophic failure of metallic glass. On the other hand, the distinct plasticity in the $x = 5$–17.5 alloys is suggested to originate from the inhomogeneous crystallization of the glassy phase during deformation. With the propagation of the shear band associated with localized viscous flow, structural segregation and transformation are induced owing to the rise of local temperature[27] or the change in the chemical short-range order (CSRO) in the metallic glasses in the less stable supercooled liquid state. The precipitation of NC particles suppresses further shear-band propagation, resulting in the arrangement of nanocrystals along with the stationary shear band. The stress concentration in the surroundings of the NC-bands activates a new shear band nucleation, and nanocrystallization occurs again during its propagation. This repeating process is tracked as the NC-band-like structure in the fracture surface of a deformed sample by TEM observation. The interaction of multiple shear bands generated as a result of the deformation-induced NC prevents the premature failure of the specimen and, thus, large plasticity is

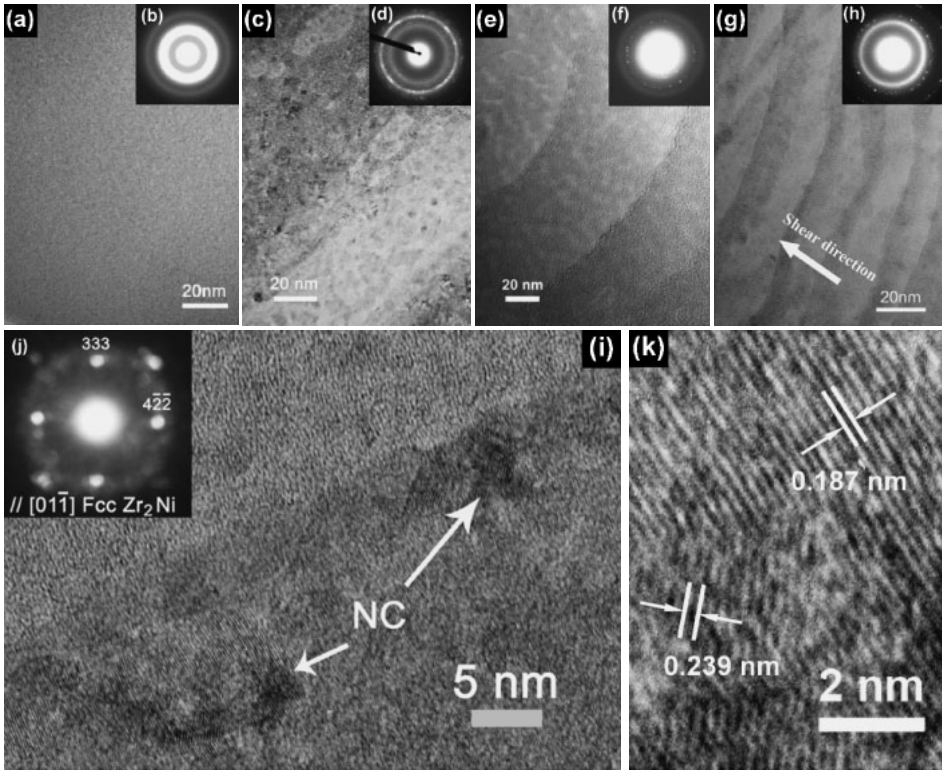

Fig. 4 High-resolution TEM (HREM) images and selected-area diffraction patterns (SADPs) taken from the fracture surface of BMGs with $x = 0$ ((a), (b)), 5 ((c), (d)), 10 ((e), (f)) and 17.5 ((g), (h)). Magnified HREM images ((i), (k)) and nanobeam electron diffraction (NBD) pattern (j) taken from the fracture surface of BMG with $x = 5$.

achieved. Finally, we confirm a tendency that the width of NC band and the distance between NC bands decrease with an increase of Pd concentration, which suggests a correlation between the behavior of the present deformation-induced nanocrystallization and the stability of supercooled liquid state in the alloys. However, the morphology of NC bands would not significantly affect the mechanical properties.

3.3 Mechanical properties of *in-situ* nano-QC formed Zr-Al-Ni-Cu-Pd BMGs

It is well known that nano-quasicrystals form as a primary phase during the devitrification of the glassy phase in the $Zr_{65}Al_{7.5}Ni_{10}Cu_{17.5-x}Pd_x$ alloy system.[28] Accordingly, the precipitation of the nano-QC phase within the glassy matrix can be achieved easily by controlling the annealing conditions. This, so far, has been established for the fabrication of QC/metallic-glass nanocomposites.[20,21,29,30] Considering that nanocrystals can also be precipitated dynamically upon deformation in the alloys with $x = 5$–17.5, we can expect the synergistic effect of nano-QC precipitation and the deformation-induced nanocrystallization for the improvement of mechanical property in the alloy system.

For the purpose of the above-stated effect, we prepared two kind of nano-QC-formed $Zr_{65}Al_{7.5}Ni_{10}Cu_{7.5}Pd_{10}$ BMGs under different annealing conditions of 680 K–360 s and 690 K–300 s. The volume fraction (V_f) of the QC phase was estimated to be 6 vol% (680 K–360 s) and 18 vol% (690 K–300 s) by evaluating the enthalpy of the first exothermic peak in the DSC curves. Figure 5 shows the results of TEM observation of the BMG with 6 vol% of the QC phase (680 K–360 s). The bright-field (BF) image (Fig. 5(a)) indicates the precipitation of particles ~10 nm in diameter homogeneously distributed within the matrix. The HREM image shown in Fig. 5(b) also contains a fringe contrast region in the glassy maze contrast. Analyses by Fast-Fourier transform reveal a fivefold symmetry of the icosahedral structure for the particle ("X"-region) and a halo pattern for the matrix ("Y"-region), confirming the dispersion of nano-scale QC precipitates within the glassy phase. The engineering S-S curves of the annealed samples with V_f of 6 and 18 vol% are shown in Fig. 6. The yield strength and Young's modulus are 1620 MPa and 98 GPa, respectively, in the nano-QC-formed BMG with V_f of 6 vol% with remaining plasticity (5.1%). The yield strength and Young's modulus clearly increase compared with those (1501 MPa and 85 GPa, respectively) of the as-cast BMG. In the BMG containing a larger amount of the QC phase (18 vol%), however, the increases in yield strength and Young's modulus (1740 MPa and 101 GPa, respectively) are accompanied by a drastic decrease in plastic strain (0.4%). The results obtained indicate that the improvement of mechanical strength and Young' modulus can be achieved without a significant loss of plasticity in the QC/glass-nanocomposite Zr-Al-Ni-Cu-Pd BMGs with the appropriate volume fraction of the QC phase.

4. Discussion

4.1 Investigation of synergistic effect of *in-situ* nano-QC formation and deformation-induced nanocrystallization

As described in 3.2, the as-cast Zr-Al-Ni-Cu-Pd BMGs exhibit significant plasticity, which originates from the

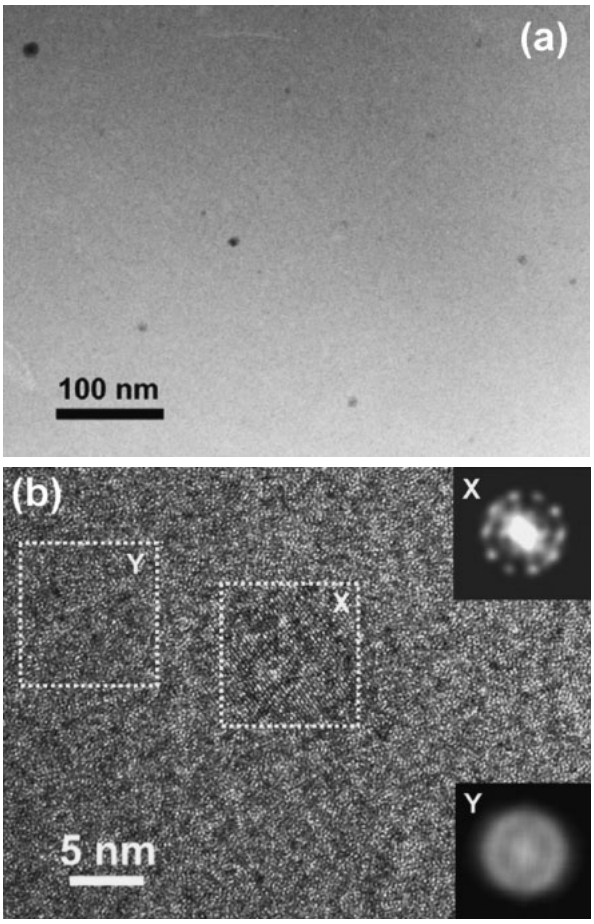

Fig. 5 Bright-field (a) and HREM (b) images of $Zr_{65}Al_{7.5}Ni_{10}Cu_{7.5}Pd_{10}$ BMG with 6 vol% of the QC phase (680 K–360 s). The HREM image also includes Fast-Fourier transforms corresponding to "X"- and "Y"-regions.

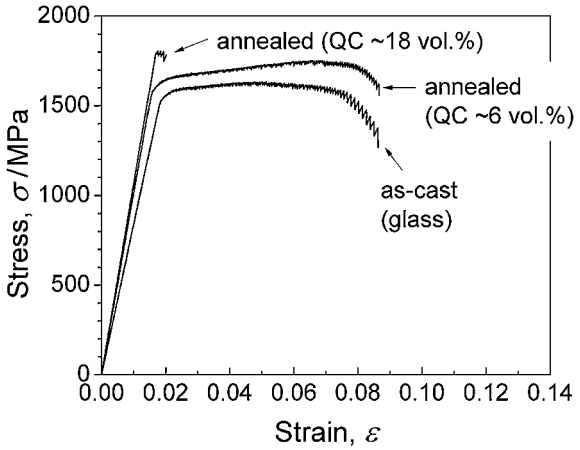

Fig. 6 Engineering stress-strain (S-S) curves of annealed $Zr_{65}Al_{7.5}Ni_{10}Cu_{7.5}Pd_{10}$ BMG with V_f of 6 and 18 vol%.

suppression of shear band propagation by deformation-induced nanocrystallization. Therefore, we expect a similar effect for the nano-QC phase dispersed BMGs, when the volume fraction of the QC phase is not very high. In the present study, it is found that plasticity remains after quasicrystallization to the volume fraction of $V_f = 6\%$, suggesting the occurrence of dynamic nanocrystallization. Actually, we can confirm a unique structure of a band-like

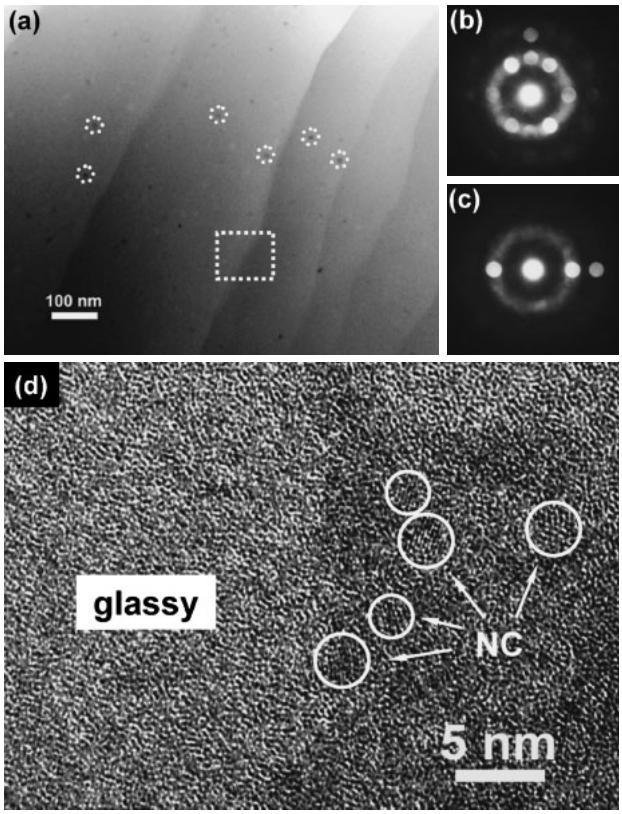

Fig. 7 Bright-field image (a), typical NBD patterns ((b), (c)) taken from the dispersed particles (within dashed circles in (a)) and magnified HREM image (d) (the vicinity of the band boundary denoted by dashed rectangle in (a)) of the fractured surface of the $Zr_{65}Al_{7.5}Ni_{10}Cu_{7.5}Pd_{10}$ BMG with V_f of 6 vol%.

pattern in addition to the dispersed particles, in the bright-field image of the fracture surface of the annealed sample after deformation, as shown in Fig. 7(a). Since typical NBD patterns taken from the dispersed particles (within dashed circles in Fig. 7(a)) are identified to have the twofold-like quasiperiodic symmetry of the icosahedral quasicrystalline phase, as displayed in Figs. 7(b) and (c), it is recognized that they are formed by annealing before deformation. Figure 7(d) shows a magnified HREM image of the vicinity of the band boundary, denoted by the dashed rectangle in Fig. 7(a). It is apparent that nanocrystalline (NC) particles ~5 nm in diameter mostly occupy the dark region near the boundary, while a glassy structure is observed in the area far from it in the bright region in Fig. 7(a). The image is consistent with those of the fracture surface of the as-cast Zr-Al-Ni-Cu-Pd BMGs. The results lead to the conclusion that the structure of the band consists of a unique mixture phases with inhomogeneous NC dispersion at the boundary and with the nano-QC particles homogeneously distributed in the glassy matrix. On the basis of the previous discussion, it is inferred that the precipitated NC particles have an fcc-Zr_2Ni structure.

4.2 Optimization of nano-QC/glassy structure for synergistic effect on mechanical properties

From the results described above, we can identify two features in the structure of the deformed sample of $Zr_{65}Al_{7.5}Ni_{10}Cu_{7.5}Pd_{10}$ BMG: (1) nano-QC particles precipi-

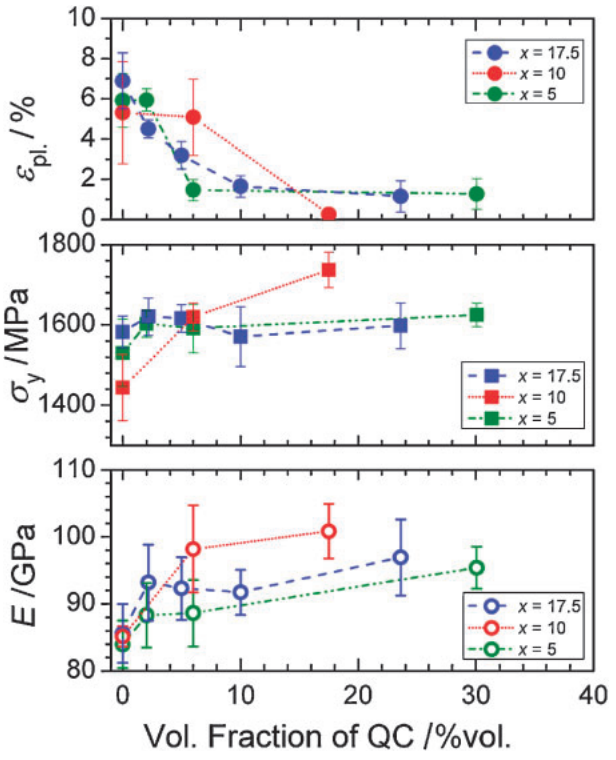

Fig. 8 Change in plastic strain (ε_{pl}), yield strength (σ_y) and Young's modulus (E) with volume fraction of QC phase in $Zr_{65}Al_{7.5}Ni_{10}Cu_{17.5-x}Pd_x$ BMGs with Pd concentrations of $x = 5$, 10 and 17.5.

tated as a result of pre-annealing, and (2) nanocrystals (with fcc-Zr_2Ni structure) induced during deformation. The two features contribute to the increase in strength and the maintenance of distinct plasticity, respectively. We have reported that the deformation-induced nanocrystallization that afforded the significant ductility is exhibited for a wide range of Pd concentration of $x = 5$–17.5 in the $Zr_{65}Al_{7.5}Ni_{10}Cu_{17.5-x}Pd_x$ BMGs. Moreover, the plasticity is almost the same for all alloy compositions. In this section, we attempt to optimize the alloy composition and the QC precipitation to obtain high mechanical strength and good ductility. Figure 8 summarizes the change in the plastic strain (ε_{pl}), yield strength (σ_y) and Young's modulus (E) with the volume fraction of the QC phase in the $Zr_{65}Al_{7.5}Ni_{10}Cu_{17.5-x}Pd_x$ BMGs with Pd concentrations of $x = 5$, 10 and 17.5. The significant increase in the yield strength from 1501 to 1740 MPa with increasing QC volume fraction (0 to 18 vol%) can be observed in the $x = 10$ alloy. Other alloys also show an increase in σ_y with increasing QC volume fraction to approximately 4 vol%, however, it is slightly less than that in the $x = 10$ alloy and it is almost constant in the QC fraction over 6 vol%. The drop in plasticity upon QC precipitation takes place in all alloys, particularly the $x = 5$ alloy, in which the plastic strain decreases drastically from 6.0 to 1.5% with QC precipitation to 6 vol%. Although the plasticity also drops to 3.2% with the QC volume fraction of 5 vol% in the $x = 17.5$ alloy, the rate of drop is lower than that in the $x = 5$ alloy. In contrast, it is noted that the plastic strain considerably maintains at 5% in the $x = 10$ alloy with a QC volume fraction less than 6 vol%. The change in Young's modulus shows a similar tendency in all alloys, indicating that it increases with QC precipitation.

Considering that the QC phase is hard and brittle, the mechanical properties of BMG strongly depend on the size as well as the volume fraction (or number) of the QC particles. Generally, the volume fraction and size of QCs should be kept low and small, respectively, to avoid a drastic drop in plasticity. In the present results, we found that a synergistic effect by nano-QC precipitation upon static annealing and deformation-induced dynamic nanocrystallization to obtain high strength and good plasticity is achieved by optimizing the alloy composition (10 at% Pd) and volume fraction of QC (less than 6%) in the $Zr_{65}Al_{7.5}Ni_{10}Cu_{17.5-x}Pd_x$ BMGs. We have already reported that the size and number of precipitated QC particles strongly depend on the Pd concentration in the $Zr_{65}Al_{7.5}Ni_{10}Cu_{17.5-x}Pd_x$ metallic glasses.[31] The Pd element plays a dominant role in the increase in the nucleation rate and the decrease in the grain growth rate of the primary precipitation of the QC phase. The nucleation and grain growth rates of the QC phase in the $Zr_{65}Al_{7.5}Ni_{10}Cu_{7.5}Pd_{10}$ metallic glass, for example, are in the order of $10^{20}/m^3$ s and 10^{-9} m/s, respectively. These values are 10^4 and 10^{-1} times those in the non-Pd-containing $Zr_{65}Al_{7.5}Ni_{10}Cu_{17.5}$ metallic glass, respectively. Consequently, the size of the QC particles decreases and their number increases drastically with increasing Pd concentration. Actually, the size of the precipitated QC phase is very fine in the $Zr_{65}Al_{7.5}Ni_{10}Cu_{7.5}Pd_{10}$ BMG, being less than 10 nm in diameter, as shown in Fig. 5. On the basis of this investigation, the Pd content of 10 at% is found to be effective for retaining plasticity via the precipitation of fine QC particles, which results in the restraint of the concentration of applied stress during deformation as well as a brittle transition owing to quasicrystallization. The present results also indicate that excess precipitation of the QC phase over 6 vol% leads to a loss of ductility, even if the grain size is fine. The details of the reason for the loss of plasticity in the alloy with the highest Pd content (17.5%) with the low QC fraction of 5 vol% are not cleared, however, it is speculated that shear band propagation, which contributes to dynamic nanocrystallization, becomes difficult because of the excess number of QC fine particles based on the highest nucleation rate in the alloy system. Even in this case, significant plasticity over 3% can be obtained when the QC volume fraction is less than 5 vol%. The mechanical properties of the present alloys and some of previously reported nano-QC/glass composites are summarized in Table 2.[20,21,29,30,32] The yield strength in this work is almost the same or slightly lower than those of other QC/glass composites with a high QC volume fraction, while the plastic strain is much improved compared with those in the previous studies. Considering that all the previous QC/glass composites with high QC volume fraction exhibit poor plasticity of less than 1% plastic strain and that little is known about the method of the improvement of plasticity in these QC/glass composites, the present results can be noted from the viewpoint of proposing new ductile BMG nanocomposites. We can, therefore, conclude that the optimization of the composition and structure in order to induce a combination of two effects of *in-situ* homogeneous nano-QC

Table 2 Mechanical properties of QC/metallic glass composites developed in this work and those reported so far.

Alloy	QC content (vol%)	Yield strength, σ_y (MPa)	Plastic strain, ε_{pl} (%)	Young's Modulus, E (GPa)	Ref.
$Zr_{57}Ti_5Cu_{20}Ni_8Al_{10}$	14	1556	0.7	71	29)
	50	1673	0.6	72	29)
$Zr_{65}Al_{7.5}Ni_{10}Cu_{7.5}Pd_{10}$	~80	1780	1.1	88	20)
$Zr_{65}Al_{7.5}Ni_{10}Cu_{12.5}Ag_5$	45	1650	0.2	85	21)
$Zr_{58}Al_9Ni_9Cu_{14}Nb_{10}$	90	1850	~0	92	30)
$(Zr_{65}Al_{7.5}Cu_{27.5})_{90}Ti_{10}$	~100	1875	~0	93	32)
$Zr_{65}Al_{7.5}Ni_{10}Cu_{12.5}Pd_5$	2	1603	5.9	88	This work
	6	1591	1.5	89	This work
	30	1625	1.3	95	This work
$Zr_{65}Al_{7.5}Ni_{10}Cu_{7.5}Pd_{10}$	6	1620	5.1	98	This work
	18	1740	0.4	101	This work
$Zr_{65}Al_{7.5}Ni_{10}Pd_{17.5}$	2	1621	4.5	93	This work
	5	1616	3.2	92	This work
	10	1589	1.7	92	This work
	24	1600	1.2	97	This work

formation and deformation-induced inhomogeneous nanocrystallization is recognized as a new technique for the production of BMGs with high strength and good ductility. The marked improvement in the mechanical properties obtained in the optimized BMG alloy of $Zr_{65}Al_{7.5}Ni_{10}Cu_{7.5}Pd_{10}$ with the QC volume fraction of 6 vol% is summarized below.

(1) Mechanical strength and Young's modulus are improved by 10% compared with those of as-cast alloy.
(2) Plastic strain remains at 5%, which is almost the same as that in the as-cast alloy and approximately 5 times that of the QC-based metallic glass with the QC volume fraction of ~80 vol%.

5. Conclusions

We have investigated the material design tailoring of the synergistic effect of *in-situ* homogeneous nano-QC formation and deformation-induced inhomogeneous nanocrystallization on mechanical strength and ductility in the $Zr_{65}Al_{7.5}Ni_{10}Cu_{17.5-x}Pd_x$ BMGs. The as-cast $Zr_{65}Al_{7.5}Ni_{10}Cu_{17.5-x}Pd_x$ ($x = 5$–17.5) BMGs exhibit significant plasticity, owing to the deformation-induced dynamic nanocrystallization. We suggest that an inhomogeneous nanoscale dynamic transformation occurs as a result of local heating or a change in CSRO during shear band propagation in Pd-containing BMGs, leading to the precipitation of nanocrystals in a band-like arrangement. It is also correlated with the lower stability of the supercooled liquid state in the alloys. The yield strength and Young's modulus increase in the nano-QC-formed $Zr_{65}Al_{7.5}Ni_{10}Cu_{17.5-x}Pd_x$ ($x = 5$–17.5) BMGs prepared by static annealing. In particular, the $Zr_{65}Al_{7.5}Ni_{10}Cu_{7.5}Pd_{10}$ BMG shows a significant increase in those properties. The drop of plasticity with nano-QC precipitation is observed in all alloys. However, it is noted that the plastic strain essentially remains at approximately 5% in the alloy with 10 at% Pd and the QC volume fraction of less than 6%. The results indicate that the improvement of mechanical strength without a loss of significant plasticity can be achieved by optimizing the alloy composition and controlling the nanostructure in the present Pd-containing alloys with a low volume fraction of the QC phase. Such good mechanical properties originate from the combination of two different features of the nanostructure in BMGs through static and dynamic control. Finally, the present method is recognized to be a new technique for the production of BMGs with high strength and good ductility.

Acknowledgements

This work was supported by Grant-in-Aid of the Ministry of Education, Culture, Sports, Science and Technology, Japan, Scientific Research (B) and Priority Area on "Science and Technology of Microwave-Induced, Thermally Non-Equilibrium Reaction Fields", and Japan Science Promotion Society (JSPS) "Asian Core Program".

REFERENCES

1) M. F. Ashby and A. L. Greer: Scr. Mater. **54** (2006) 321–326.
2) A. Inoue and N. Nishiyama: MRS Bull. **32** (2007) 651–658.
3) J. Schroers and W. L. Johnson: Phys. Rev. Lett. **93** (2004) 255506-1-4.
4) D. V. Louzguine-Luzgin, A. Vinogradov, A. R. Yavari, S. Li, G. Xie and A. Inoue: Philos. Mag. **88** (2008) 2979–2987.
5) J. Das, M. B. Tang, K. B. Kim, R. Theissmann, F. Baier, W. H. Wang and J. Eckert: Phys. Rev. Lett. **94** (2005) 205501-1-4.
6) K. B. Kim, J. Das, S. Venkataraman, S. Yi and J. Eckert: Appl. Phys. Lett. **89** (2006) 071908-1-3.
7) L. Y. Chen, A. D. Setyawan, H. Kato, A. Inoue, G. Q. Zhang, J. Saida, X. D. Wang, Q. P. Cao and J. Z. Jiang: Scr. Mater. **59** (2008) 75–78.
8) Q. Murali and U. Ramamurty: Acta Mater. **53** (2005) 1467–1478.
9) A. H. Brothers and D. C. Dunand: Adv. Mater. **17** (2005) 484–486.
10) A. Inoue, T. Wada and D. V. Louzguine-Luzgin: Mater. Sci. Eng. A **471** (2007) 144–150.
11) C. C. Hays, C. P. Kim and W. L. Johnson: Phys. Rev. Lett. **84** (2004) 2901–2904.
12) D. C. Hofmann, J. Y. Suh, A. Wiest, G. Duan, M. L. Lind, M. D. Demetriou and W. L. Johnson: Nat. **451** (2008) 1085–1089.
13) H. Kato, T. Hirano, A. Matsuo, Y. Kawamura and A. Inoue: Scr. Mater. **43** (2000) 503–507.
14) M. E. Siegrist and J. F. Löffler: Scr. Mater. **56** (2007) 1079–1082.
15) H. C. Yim and W. L. Johnson: Appl. Phys. Lett. **71** (1997) 3808–3810.

16) J. Saida, A. D. H. Setyawan, H. Kato and A. Inoue: Appl. Phys. Lett. **87** (2005) 151907-1-3.
17) S. W. Lee, M. Y. Huh, E. Fleury and J. C. Lee: Acta Mater. **54** (2006) 349–355.
18) G. Kumar, T. Ohkubo, T. Mukai and K. Hono: Scr. Mater. **57** (2007) 173–176.
19) J. Saida, A. D. Setyawan, H. Kato, M. Matsushita and A. Inoue: Mater. Trans. **49** (2008) 2732–2736.
20) A. Inoue, T. Zhang, M. W. Chen, T. Sakurai, J. Saida and M. Matsushita: Appl. Phys. Lett. **76** (2000) 967–969.
21) A. Inoue, T. Zhang, M. W. Chen, T. Sakurai, J. Saida and M. Matsushita: J. Mater. Res. **15** (2000) 2195–2208.
22) A. D. Setyawan, H. Kato, J. Saida and A. Inoue: J. Appl. Phys. **103** (2008) 044907-1-8.
23) W. F. Wu, Y. Li and C. A. Schuh: Philos. Mag. **88** (2008) 71–89.
24) A. Inoue, T. Zhang, N. Nishiyama, K. Ohba and M. Matsumoto: Mater. Trans. JIM **34** (1993) 1234–1237.
25) Z. Altounian, E. Batalla, J. O. Strom-Olsen and W. L. Walter: J. Appl. Phys. **61** (1987) 149–155.
26) J. Saida, M. Matsushita and A. Inoue: Intermetallics **10** (2002) 1089–1098.
27) J. J. Lewandowski and A. L. Greer: Nat. Mater. **5** (2006) 15–18.
28) A. Inoue, T. Zhang, J. Saida, M. Matsushita, M. W. Chen and T. Sakurai: Mater. Trans. JIM **40** (1999) 1137–1143.
29) L. Q. Xing, J. Eckert, W. Löser and L. Schultz: Appl. Phys. Lett. **74** (1999) 664–666.
30) J. B. Qiang, W. Zhang, G. Q. Xie, H. Kimura, C. Dong and A. Inoue: Intermetallics **15** (2007) 1197–1201.
31) J. Saida, M. Matsushita and A. Inoue: Mater. Trans. JIM **41** (2000) 1505–1510.
32) J. B. Qiang, W. Zhang, G. Q. Xie and A. Inoue: Mater. Trans. **48** (2007) 1789–1792.